Progress In Electromagnetics Research M, Vol. 120, 95–111, 2023

Wearable Dual-Band Frequency Reconfigurable Patch Antenna for WBAN Applications

Umar Musa[1], Shaharil Mohd Shah[1, *], Huda A. Majid[1], Mohamad K. A. Rahim[2], Muhammad Sani Yahya[3], Zainab Yunusa[4], Abubakar Salisu[5], and Zuhairiah Zainal Abidin[1]

Abstract—A wearable dual-band patch antenna is presented which can adjust its frequency for WBAN applications. Frequency reconfiguration is achieved by the antenna through the utilization of the switching properties of a PIN diode. Produced using a Rogers Duroid material with semi-flexible properties, the antenna has a size of $0.33\lambda_0 \times 0.35\lambda_0 \times 0.012\lambda_0$. Initially resonating at 5.8 GHz, a slot in the shape of an inverted letter U is included to introduce a dual-band operation at 2.4 GHz. By controlling the PIN diode's ON and OFF states, the antenna can switch between single-band (ISM 5.8 GHz) and dual-band (ISM 2.4 GHz and 5.8 GHz) operations. The antenna exhibits a bi-directional radiation pattern at 2.4 GHz and a directional pattern at 5.8 GHz. In the ON state, the antenna achieves a peak gain and total efficiency of 4.84 dBi, 5.87 dBi, 92.5%, and 92.7% at 2.4 GHz and 5.8 GHz, respectively. In the OFF state at 5.8 GHz, a peak gain and total efficiency of 6.01 dBi and 91.8% are measured. To evaluate its suitability for WBAN applications, the antenna's performance is assessed by measuring SAR values on a human tissue model. At 2.4 GHz, the SAR values for 1/10 g of human tissue are 0.411/0.177 W/kg respectively. Similarly, at 5.8 GHz, the SAR values are 0.438/0.158 W/kg respectively. The SAR values comply with the established standards of the FCC and ICNIRP for both resonance frequencies for human tissue weighing 1/10 g. Overall, the antenna boasts a compact size, acceptable SAR values, and satisfactory gain and efficiency across all operating bands, surpassing previous works. It also benefits from a simplified design employing a single switch, and the antenna remains a suitable choice for WBAN applications considering its other advantageous characteristics mentioned above.

1. INTRODUCTION

The utilization of body-centric wireless communication has significantly grown in recent times due to the fast-paced advancement of wireless technology. Wireless Body Area Network (WBAN) is a grouping of wireless devices operating near the human body [1]. For wearable devices to be effective, they need to be functional, comfortable to wear, non-intrusive, and unobstructed. WBANs have found widespread applications in a wide range of fields, including healthcare services, entertainment, sporting events, and military applications [2]. Among the most important aspects of current healthcare is tracking patients' condition, including temperature, blood pressure, and heart rate [3]. WBAN network communication lines are divided into three distinct states depending on the sensor's (antenna's) position whether it is located inside or on different regions of the human body, namely in-, on-, or off-body [4].

Received 7 June 2023, Accepted 17 July 2023, Scheduled 26 October 2023

* Corresponding author: Shaharil Mohd Shah (shaharil@uthm.edu.my).

[1] Advanced Telecommunication Research Center (ATRC), Universiti Tun Hussein Onn Malaysia (UTHM), Parit Raja, Johor 86400, Malaysia. [2] Faculty of Electrical Engineering, Universiti Teknologi Malaysia (UTM), 81310, Malaysia. [3] Universiti Teknologi PETRONAS,, Seri Iskandar 32610, Malaysia. [4] Department of Electrical Engineering, University of Hafr Al Batin Hafr Al Batin, Saudi Arabia. [5] Department of Electronics and Biomedical Engineering, University of Bradford, United Kingdom.

The emphasis is placed on on-body communication in WBAN, in which an antenna located on the body connects with a device located off the body. As a result, a small antenna with directional radiation and a few back lobes is required for that purpose [5]. The antennas integrated into the human body must uphold their operational capabilities concerning bandwidth, frequency, gain, and efficiency, while simultaneously adhering to specified regulations like the limits for Specific Absorption Rate (SAR) [6, 7]. So far, from the previous literature, the antennas of interest have a limited operating band. As a result, multiple single-frequency antennas are used and thereby, increasing space usage, cost of fabrication, system complexity, intermodulation distortion, and limitations to be applied on wearable devices. Furthermore, a fixed multiband antenna can only operate at a limited number of frequencies. A wearable versatile antenna capable of reconfiguration and operation across multiple frequency bands, as well as being adaptable to various parts of the human body, is then very much preferred [8].

The term reconfigurability refers to the capability of a wearable antenna to modify its radiation pattern, frequency, and polarization to suit different applications. For users' comfort, these antennas must be wearable and lightweight. They must also be able to withstand severe operating conditions as well as on-body deformations such as bending or tearing [9, 10]. Rather than employing multiple antennas at various frequencies for signal transmission and reception, frequency reconfigurable antennas are designed to achieve this goal by improving the antenna's functionality [11].

There have been numerous reports in recent years on frequency-reconfigurable antennas that use active switches like PIN diodes, varactors, and radio frequency micro-electromechanical system (RF MEMS) [12–14]. Typically constructed on a rigid substrate, these antennas have the ability to change their configuration with respect to resonant frequencies [15–18], radiation patterns [19–21], and polarization [22–25]. However, these designs are rigid, and they transmit all resonances despite user requirements. Alternatively, a single wearable antenna with different resonant frequencies is preferred. On the other hand, the number of wearable antennas that are practically frequency reconfigurable is limited based on the open literature. The primary cause for this difficulty lies in the challenges associated with establishing durable electrical and mechanical connections within stationary electronic parts and bendable conductors [26].

Prior investigations have uncovered a few frequency reconfigurable antennas that are suitable for use in WBAN applications. For instance, the work in [27] designs a low-weight antenna suitable for WBAN applications to suit various frequencies. The antenna utilized in the study is a circular radiator with stub-loading, implemented on a Rogers RT5880 material, with a height of 0.254 mm. To enable frequency reconfigurability, the antenna design integrated a pair of PIN diodes. As a result, the antenna possesses the capability to resonate across multiple frequency bands. Similarly, a textile antenna with the capability to reconfigure its frequency was designed in [28]. To achieve frequency reconfiguration, the antenna design consisted of a rectangular patch and a defective ground structure. This design incorporated three PIN diode switches, offering seven different switch configurations. The antenna demonstrated operational capabilities at various frequencies.

A folding slot antenna with frequency reconfigurability is specifically designed for applications in WBAN [29]. A single PIN diode reconfigured the folded slot and stub antenna. The antenna functioned at 2.45 GHz and 3.3 GHz in the ON state. The antenna worked at 2.45 GHz in the OFF state. Also, the authors in [30] studied a low-profile antenna with frequency reconfigurability for WBAN applications, incorporating a PIN diode with compact dimensions of $0.14\lambda_0 \times 0.13\lambda_0 \times 0.001\lambda_0$, and it achieved multiple frequency bands.

Similarly, a frequency reconfigurable antenna operating within the Industrial, Scientific, and Medical (ISM) bands was introduced in [31]. To achieve frequency reconfiguration, two PIN diode switches were strategically placed on the ground plane. By altering the switch states, the antenna becomes capable of operating at different frequencies, namely 2.4 GHz, 3.5 GHz, 5.8 GHz, and 5.9 GHz. At these respective operating bands, the antenna exhibits peak gains of 4.93 dBi, 5.67 dBi, 8.86 dBi, and 10.07 dBi. While wearable antennas exist, they often suffer from either large size or a limited number of resonant frequencies. Furthermore, the evaluation of the antenna's flexibility and SAR analysis for wearable applications, ensuring its safe usage in close connection to human body, proved insufficient [32]. However, the utilization of a Rogers Duroid RO3003^{TM} substrate material with semi-flexible properties in this study has effectively addressed the issues of rigidity and inflexibility that were prevalent in previous wearable reconfigurable antenna designs.

This study introduces a wearable patch antenna tailored for WBAN applications. The antenna exhibits frequency reconfigurability and is initially designed to resonate at 5.8 GHz. However, to overcome the limitation of single-frequency operation, a slot in the shape of an inverted letter U is included, resulting in an additional resonance at 2.4 GHz. Furthermore, bandwidth and gain are enhanced through the inclusion of two smaller slots and a partial ground plane.

The proposed antenna uses an SMP 1321 PIN diode from Skyworks Technologies with a biasing circuit to switch between ON and OFF states, thus enabling both single-band (ISM 5.8 GHz) and dual-band (ISM 2.4 GHz and 5.8 GHz) operations. The choice of the 2.4 GHz and 5.8 GHz bands is significant for WBAN applications. The 2.4 GHz band, which is globally available for commercial use, is highly favored due to the presence of low-power communication standards like ZigBee. On the other hand, the 5.8 GHz band is well suited for high-speed mobile and radio communication, making it an ideal choice for monitoring systems, autonomous drones, automation, and other communication networks that necessitate video, voice, and data transfer. The capability to switch between these bands enables the gathering of essential information via on-body sensors and transmitting it to a control center for further data recording.

Section 2 provides a comprehensive overview of the proposed antenna's geometry, theoretical foundation, and switching techniques. Section 3 delves into the radiation characteristics of the antenna, followed by Section 4 which investigates the impact of bending. In Section 5, the antenna's behavior in proximity to the human body is scrutinized. The SAR analysis of the antenna is expounded upon in Section 6, and a comparative analysis between the proposed antenna and previous designs is presented in Table 4. Lastly, Section 7 concludes the study by providing a summary of the findings.

2. ANTENNA DESIGN AND GEOMETRY

This section provides a comprehensive description of the fundamental geometry of the proposed patch antenna which allows for frequency reconfigurability. Additionally, we examine the implementation of an equivalent circuit model, along with delving into the underlying design theory and switching techniques. To accomplish the reconfiguration of resonant frequencies, the antenna is meticulously designed and simulated in the schematic environment of CST Microwave Studio^{TM} software, utilizing lumped elements and Touchstone 2-port S-parameters or *.s2p files. However, in the practical fabrication and measurement setup, an actual SMP 1321 PIN diode sourced from Skyworks Technologies is utilized to achieve the desired reconfigurability.

2.1. Proposed Antenna Structure

Figures 1(a) and (b) depict the suggested antenna's geometry. Its geometry is designed to be compact, measuring $41 \times 44 \times 1.52\,\text{mm}^3$, corresponding to $0.33\lambda_0 \times 0.35\lambda_0 \times 0.012\lambda_0$, where λ_0 represents the free space wavelength at 2.4 GHz. Constructed on a Rogers Duroid RO3003^{TM} material, the antenna integrates a microstrip feed line and a rectangular radiating patch. This material establishes the essential groundwork for achieving optimal antenna performance, featuring key attributes such as a height of 1.52 mm, a loss tangent coefficient of 0.0013, and a dielectric constant of 3. Utilizing a frequency reconfiguration technique, the antenna can seamlessly switch between the two ISM bands of 2.4 GHz and 5.8 GHz.

2.2. Proposed Antenna Design Theory

The computation of the lengths and widths of the antenna relies on the principles of the transmission line model theory presented in [33]. Initially, the primary radiating surface resonates at 5.8 GHz. To establish a supplementary resonant frequency of 2.4 GHz, a slot that is shaped like an inverted U is incorporated. Furthermore, in order to achieve improved impedance bandwidth and gain, the patch is equipped with a partial ground plane and two additional slots, as seen in Fig. 2(a). During the initial phase of implementing the reconfigurable antenna, to investigate the antenna's characteristics, an ideal switch (copper bridge) is used with dimensions of $0.3 \times 1\,\text{mm}^2$, which is introduced across the horizontal slot on the radiating plane to have a general idea of the switching characteristics. Figs. 2(b) and (c) show the antenna design without and with a copper bridge. In Fig. 3, the reflection coefficient S_{11} of

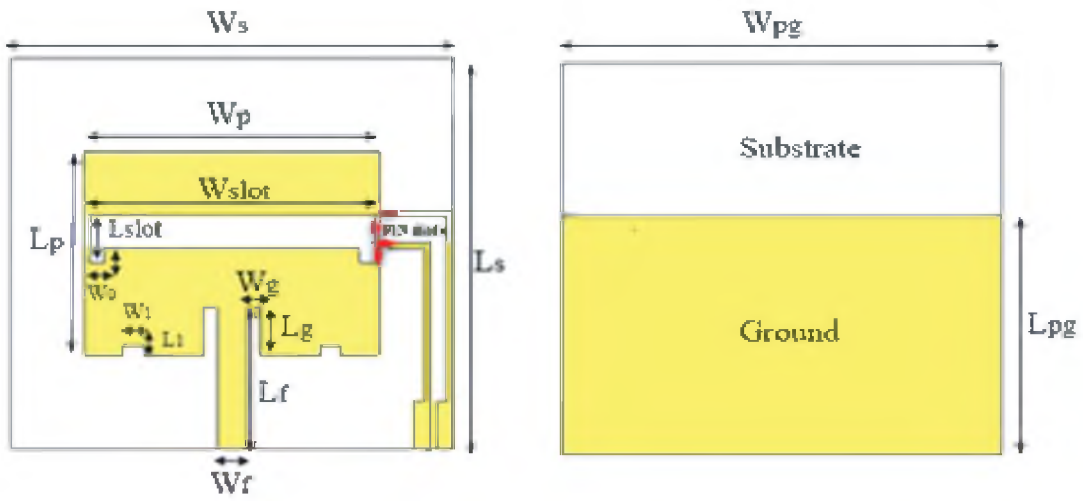

Figure 1. Antenna geometry: (a) front, (b) back. The dimensions of the antennas are $Ls = 41\,\text{mm}$, $Ws = 44\,\text{mm}$, $Wp = 29\,\text{mm}$, $Lp = 21\,\text{mm}$, $Wpg = 41\,\text{mm}$, $Lpg = 25\,\text{mm}$, $Wslot = 28\,\text{mm}$, $Lslot = 3.7\,\text{mm}$, $h = 1.52\,\text{mm}$, $Wf = 2.98\,\text{mm}$, $Lf = 15\,\text{mm}$, $Lg = 5\,\text{mm}$, $Wg = 2\,\text{mm}$, $Wo = 1.5\,\text{mm}$, $Lo = 1.4\,\text{mm}$, $W1 = 2.2\,\text{mm}$, $L1 = 1\,\text{mm}$, $Tp = 0.035\,\text{mm}$.

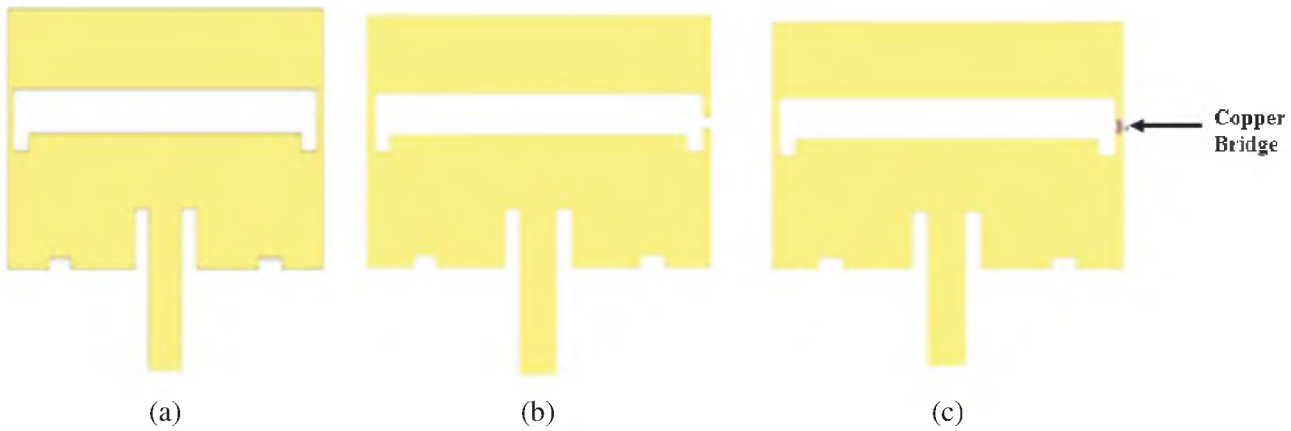

Figure 2. Proposed antenna at three design stages: (a) without a PIN diode, (b) without a copper bridge (OFF state), (c) with a copper bridge (ON state).

the antenna is depicted through simulations, both without and with a copper bridge. Table 1 exhibits the antenna's performance at various stages throughout the design process.

Table 1. Proposed antenna performance in various design stages.

Parameter	Ideal switch (ON State)		PIN Diode (ON State)		Ideal switch (OFF State)	PIN Diode (OFF State)
Freq. (GHz)	2.4	5.8	2.4	5.8	5.8	5.8
BW (%)	3.45	5.10	3.80	5.20	5.95	5.31
Gain (dBi)	3.37	4.96	4.84	5.87	5.07	5.89
Eff. (%)	91.4	91.9	92.5	92.7	92.2	91.8

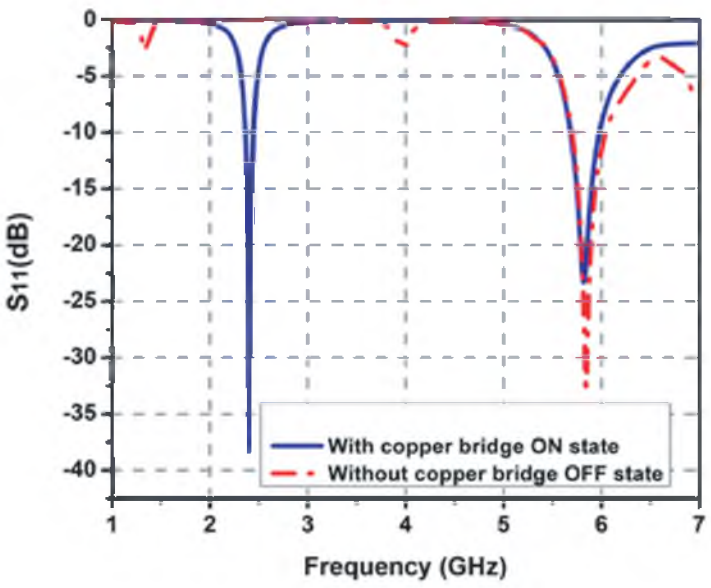

Figure 3. Simulated S_{11} of the antenna without and with a copper bridge.

2.3. PIN Diode Switching Technique

A PIN diode is chosen in this work due to its advantages compared to other active switches [34]. Prior to that, a decision is made on a suitable PIN diode from those available commercially. Skyworks Technologies' SMP1321 PIN diode is an active switch with very low capacitance (0.18 pF) with frequencies ranging from 10 MHz to 10 GHz [35]. This frequency range meets the range required in this work. A Touchstone 2-port S-parameters file (*.s2p) simulates the antenna in both states, which also includes parasitic package effects. Figs. 4(a) and (b) illustrate the schematic diagram in ON and OFF states using the *.s2p files of the SMP1321 PIN Diode in CST Microwave Studio^{TM} software. Fig. 4(c) illustrates the biasing circuit, which demonstrates that the excitation of the PIN diode is achieved through an RF choke with an inductance (L) of 27 nH and a DC blocking capacitor with a capacitance (C) of 1800 pF. The selection of the RF choke and DC blocking capacitor is based on matching the resistance of the RF line with the biased circuit. The capacitor serves to restrict the interaction of the DC biasing current with the RF signals, while the RF choke guides the DC current required for the PIN diode to function. A voltage supply of +1.1 V with a current of 0.03 A is fed from the power supply to the antenna to switch on the PIN diode which is equivalent to 15.19 dBm of DC power consumed by the PIN diode.

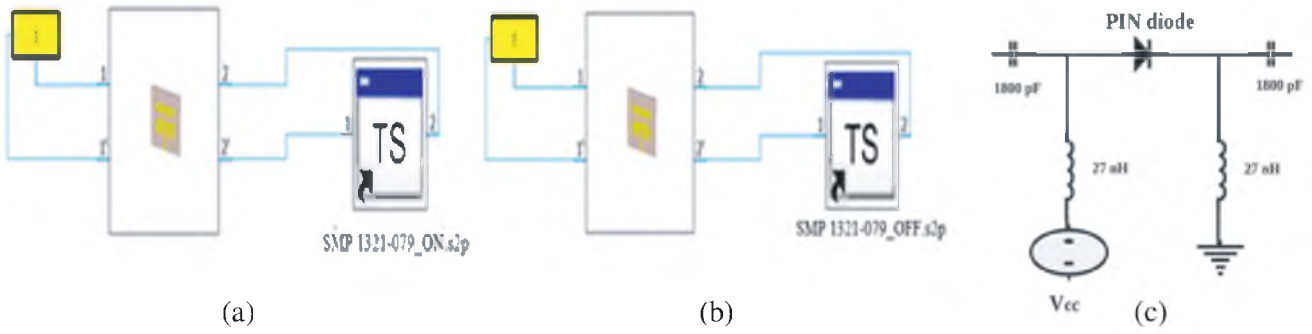

Figure 4. PIN diode schematic diagram: (a) ON state, (b) OFF state, (c) Biasing circuit.

2.4. Equivalent Circuit

The frequency reconfigurable patch antenna in this study is represented by the equivalent circuit model depicted in Fig. 5, which was implemented using the ADS (Advanced Design System) software. In Fig. 5(a), parallel lumped components symbolize the radiating patch of the antenna, specifically C1 (capacitance), R1 (resistance), and L1 (inductance). These components allow the antenna to resonate at 5.8 GHz. To determine the values of R1, L1, and C1, the equations provided in [36, 37] are employed. Additionally, the inclusion of a slot having a shape like that of an inverted U and two smaller slots in the patch enables the antenna to resonate at 2.4 GHz. Consequently, the antenna's equivalent model undergoes modifications, as seen in Fig. 5(b), where it is characterized by a sequence of inductance and capacitance values computed using the equations provided in [38, 39]. Figs. 5(c) and (d) demonstrate the PIN diode in the ON and OFF states, respectively. In the ON state, the PIN diode is configured with series resistance and inductance values of 1.05 Ω and 0.7 nH. In the OFF state, the diode is arranged in a shunt configuration with resistance and capacitance values of 2000 Ω and 0.18 pF, respectively. Mutual inductance (Lm) and mutual capacitance (Cm) are also utilized to couple the resonant circuits of the antenna, as illustrated in Fig. 5(e).

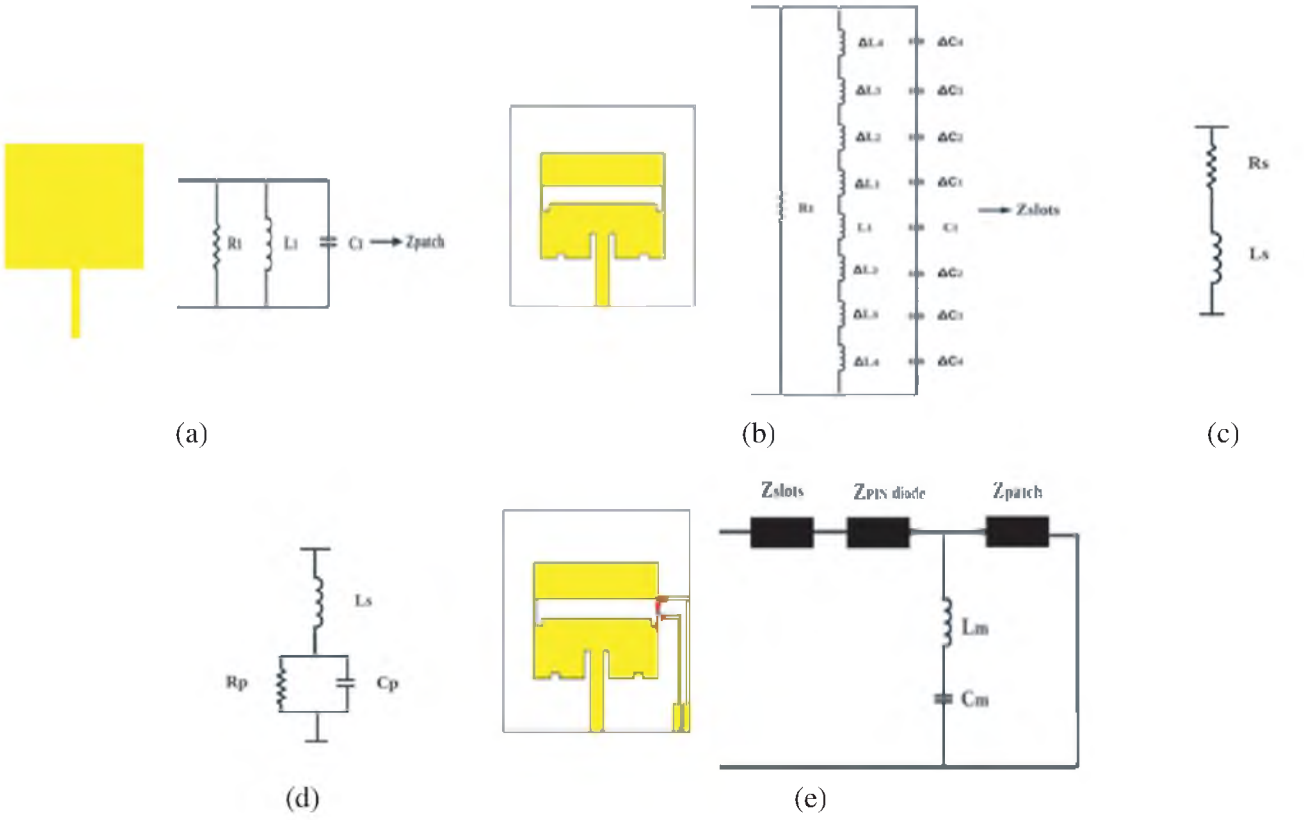

Figure 5. Equivalent circuit using ADS software: (a) main plain, (b) supplementary slots, (c) ON state, (d) OFF state, (e) proposed antenna. Values of each component in the equivalent circuit are $R1 = 49.8\,\Omega$, $L1 = 0.6\,\text{nH}$, $C1 = 3.4\,\text{pF}$, $\Delta L1 = 2.9\,\text{nH}$, $\Delta L2 = 9.4\,\text{nH}$, $\Delta L3 = 5.7\,\text{nH}$, $\Delta L4 = 7.7\,\text{nH}$, $\Delta C1 = 2.3\,\text{pF}$, $\Delta C2 = 1.6\,\text{pF}$, $\Delta C3 = 5.5\,\text{pF}$, $\Delta C4 = 0.9\,\text{pF}$, $Lm = 0.6\,\text{nH}$, $Cm = 2.9\,\text{pF}$, $Rs = 1.05\,\Omega$, $Rp = 2000\,\Omega$, $Ls = 0.7\,\text{nH}$, $Cp = 0.18\,\text{pF}$.

3. ANALYSIS OF RESULTS

For the verification of the design and simulations, a physical prototype was constructed, as depicted in Fig. 6(a). The antenna receives power through a readily available 50 Ω SMA connector. The antenna's

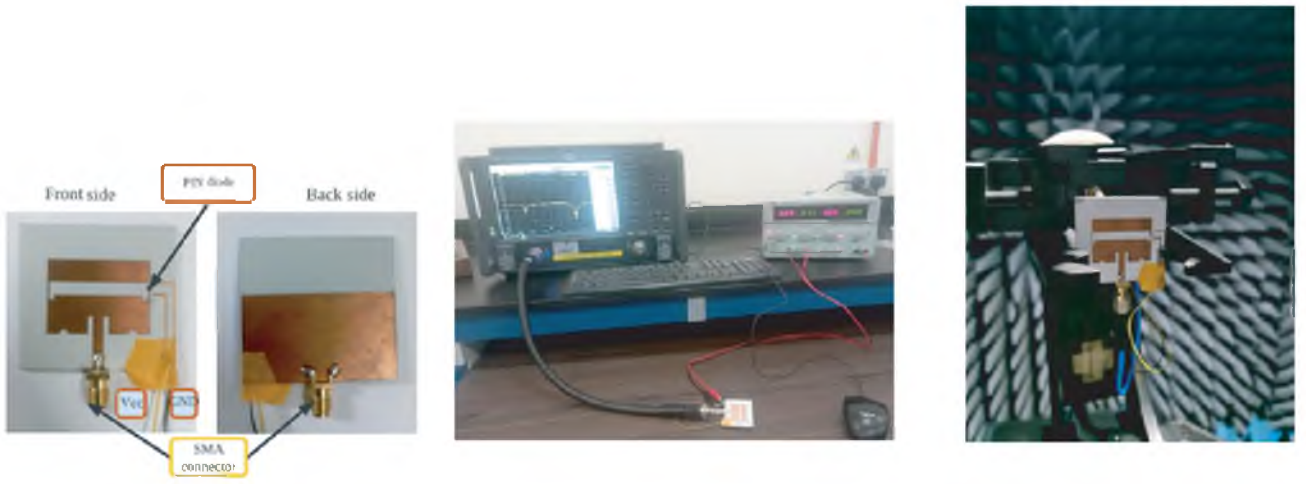

(a) (b) (c)

Figure 6. (a) Antenna prototype, (b) S_{11} measurement configuration, (c) far-field measurement configuration.

performance is assessed using a Keysight PNA-L Vector Network Analyzer (VNA) and a calibrated anechoic chamber, as illustrated in Figs. 6(b) and (c), respectively. Additionally, bending investigation and simulations of the SAR limits are carried out, and on-body measurements are conducted to confirm its suitability for WBAN applications.

3.1. Reflection Coefficient

The VNA is utilized to measure the S_{11} of the antenna being tested. In Fig. 7, a comparison is presented between the measured and simulated S_{11} values of the antenna under two states: ON and OFF. During the ON state, the antenna functions at dual-band frequencies of 2.4 GHz and 5.8 GHz. Fig. 7(a) shows that at 2.4 GHz the measured bandwidth is 3.8%, while the measured bandwidth is 5.2% in the OFF state at 5.8 GHz, and the antenna functions at a single frequency band of 5.8 GHz, exhibiting a measured bandwidth of 5.4% as depicted in Fig. 7(b). The overall comparison of the antenna's performance in the ON and OFF states is presented in Fig. 7(c). The presented figures exhibit a satisfactory level of agreement between the simulated, measured, and circuit model results.

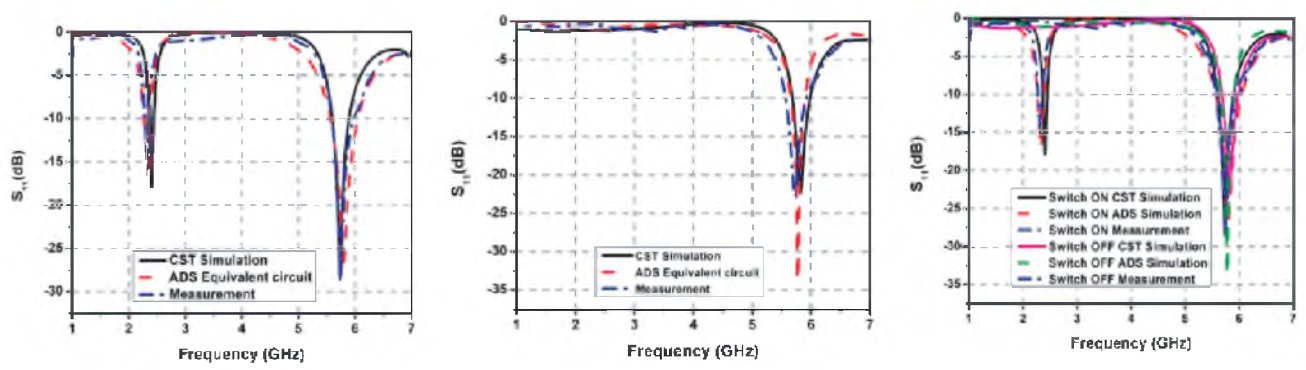

(a) (b) (c)

Figure 7. S_{11} comparison: (a) ON state, (b) OFF state, (c) ON and OFF states.

3.2. Current Distribution

The current distribution of an antenna plays a critical role in its functioning at a specific frequency. At 2.4 GHz in the ON state, Fig. 8(a) reveals that the primary concentration of current is directed toward the slot's boundaries. Conversely, at 5.8 GHz, as depicted in Fig. 8(b), most of the current is found in the center of the radiating patch. Figs. 8(c) and (d) illustrate the current distribution in the OFF state. From Fig. 8(c), it is evident that in the OFF state, no current flows across the slot's edges, contributing to the lower resonance frequency at 2.4 GHz. On the other hand, at the higher resonance frequency of 5.8 GHz, as shown in Fig. 8(d), the primary concentration of current is prominently located around the center of the main radiating patch. These findings align with the theoretical justification presented in the literature [40], which states that the resonant frequency is influenced by the length of the current path on the radiating patch. Specifically, a longer current path across the radiating patch leads to a lower resonant frequency, while a shorter path corresponds to a higher resonant frequency.

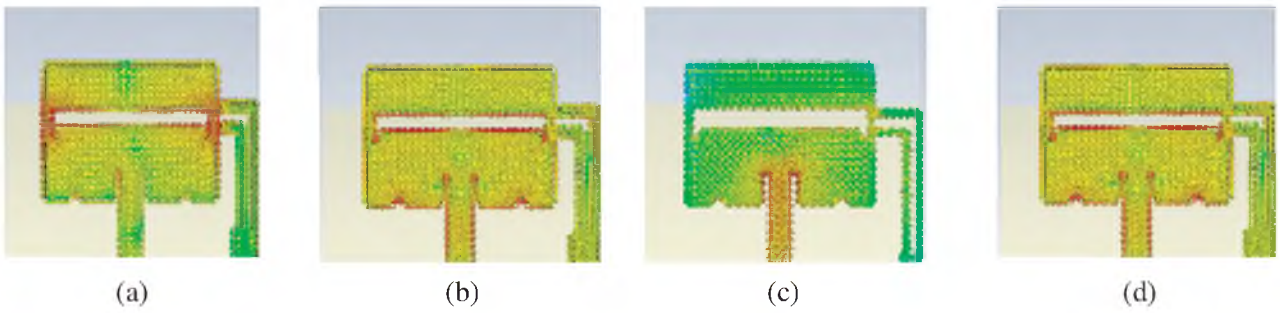

Figure 8. Current distribution: (a) 2.4 GHz (ON state), (b) 5.8 GHz (ON state), (c) 2.4 GHz (OFF state), (d) 5.8 GHz (OFF state).

3.3. Radiation Properties and Gain

The radiation properties were analyzed in both the ON and OFF states. Fig. 9 illustrates the simulated and measured 2D radiation patterns for the antenna in the ON state. In the ON state at 2.4 GHz, a bi-directional radiation pattern in the E-plane and omnidirectional radiation pattern in the H-plane are observed as depicted in Fig. 9(a). Conversely, at 5.8 GHz, a directional radiation pattern in the

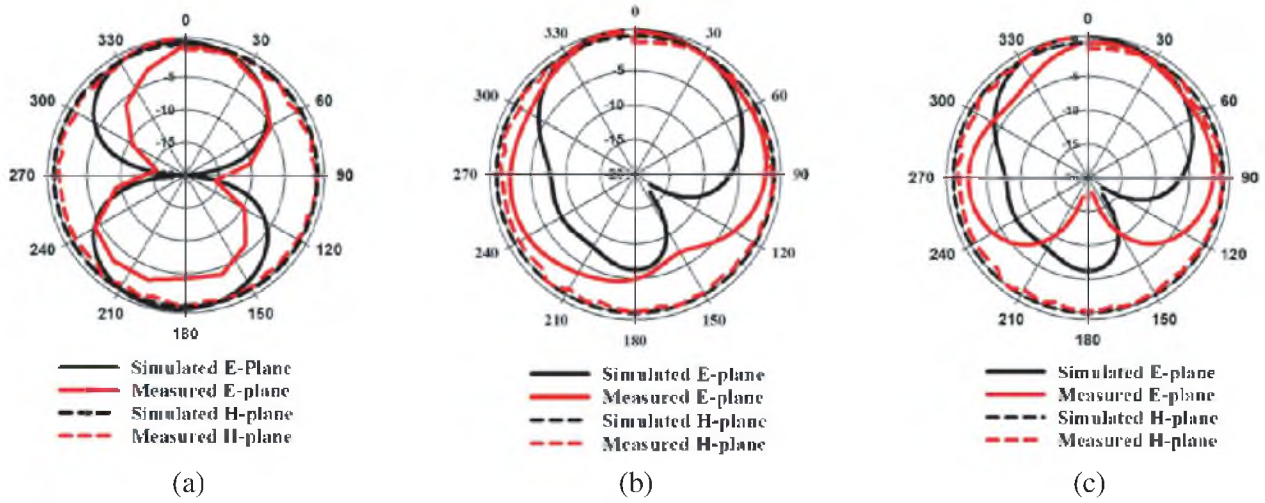

Figure 9. Radiation patterns: (a) 2.4 GHz (ON state), (b) 5.8 GHz (ON state), (c) 5.8 GHz (OFF state).

E-plane and omnidirectional radiation pattern in the H-plane are observed as depicted in Fig. 9(b). In the OFF state at 5.8 GHz, a directional radiation pattern in the E-plane and omnidirectional radiation pattern in the H-plane are observed as depicted in Fig. 9(c). The gain and efficiency values confirm that the antenna is suitable for operation in the 2.4 GHz and 5.8 GHz ISM bands. In the ON state, peak gain and total efficiencies are measured to be 5.87 dBi/92.7% and 4.84 dBi/92.5% at 5.8 GHz and 2.4 GHz, respectively, as shown in Fig. 10(a) and Fig. 10(b). In the OFF state, a peak gain and total efficiency of 6.01 dBi and 91.8% are measured at 5.8 GHz, as presented in Fig. 10(c). To further verify the results, Fig. 11 depicts the radiation characteristics (3D) corresponding to the operational bands under consideration.

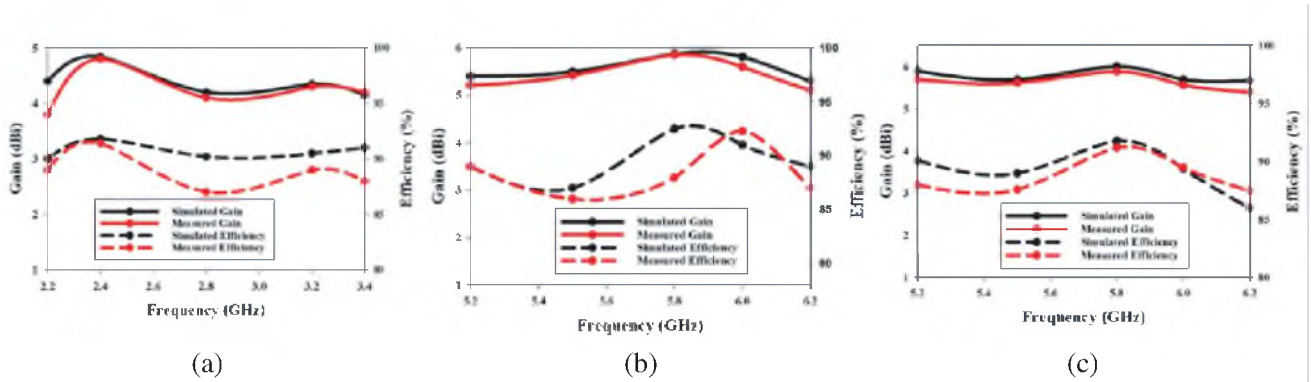

Figure 10. Relationship between Gain and efficiency: (a) 2.4 GHz (ON state), (b) 5.8 GHz (ON state), (c) 5.8 GHz (OFF state).

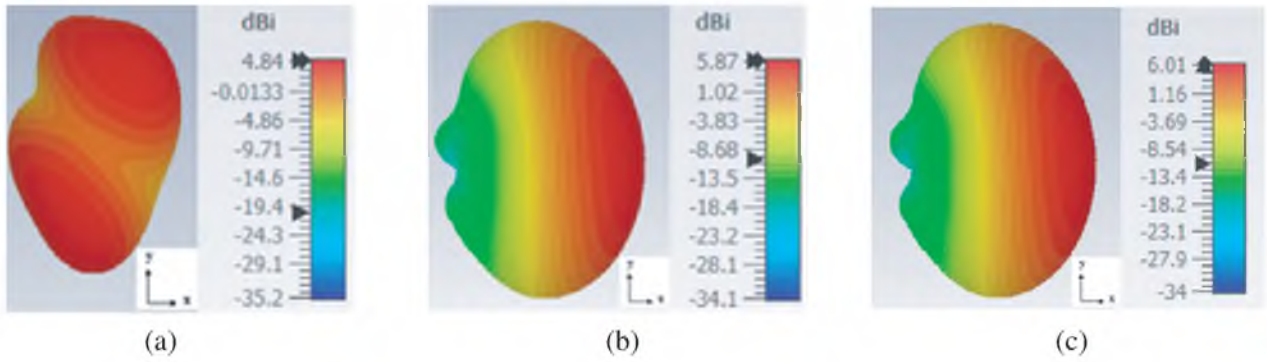

Figure 11. 3D radiation patterns: (a) 2.4 GHz (ON state), (b) 5.8 GHz (ON state), (c) 5.8 GHz (OFF state).

4. BENDING INVESTIGATION

To ensure the antenna's suitability for WBAN applications when it is applied to human body, validating its ability to adapt to specific bending radii is crucial. The investigation of bending is conducted on the x-direction and y-direction, as depicted in Figs. 12(a)–(d). The antenna's operational characteristics in the ON state, when it is subjected to deformation in both axis, are depicted in Figs. 13(a)–(d), considering various diameters measurements of (50, 80, and 100 mm). The S_{11} values for all diameters are nearly identical. Styrofoam is utilized for validation purposes while evaluating the behavior of the antenna under deformation. Figs. 14(a)–(d) depict the behavior of the antenna in the OFF state under deformations in the y- and x-directions. The S_{11} across all diameters exhibit a similar pattern, following the same behavior as in the ON state. It was noted that the simulation results exhibit significantly

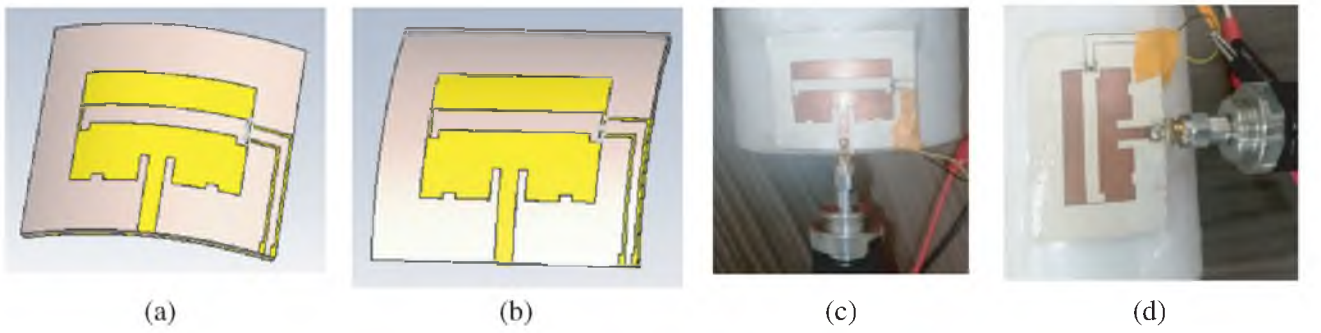

(a) (b) (c) (d)

Figure 12. Antenna in bending condition: (a) y-direction (simulation), (b) x-direction (simulation), (c) y-direction (measurement), (d) x-direction (measurement).

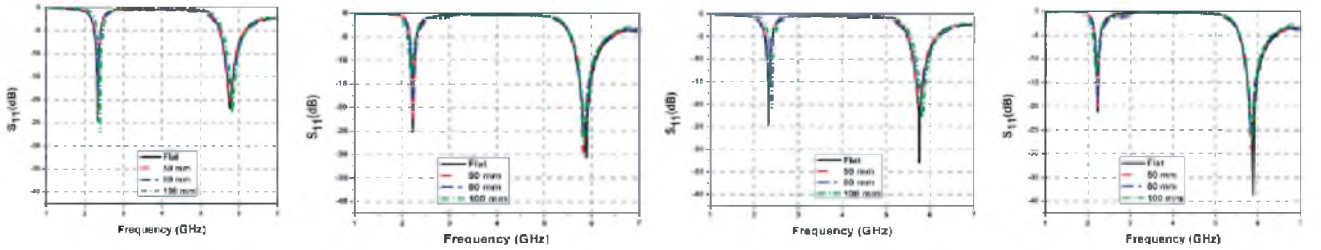

(a) (b) (c) (d)

Figure 13. S_{11} under bending condition: (a) y-direction ON state (simulation), (b) y-direction ON state (measurement), (c) x-direction ON state (simulation), (d) x-direction ON state (measurement).

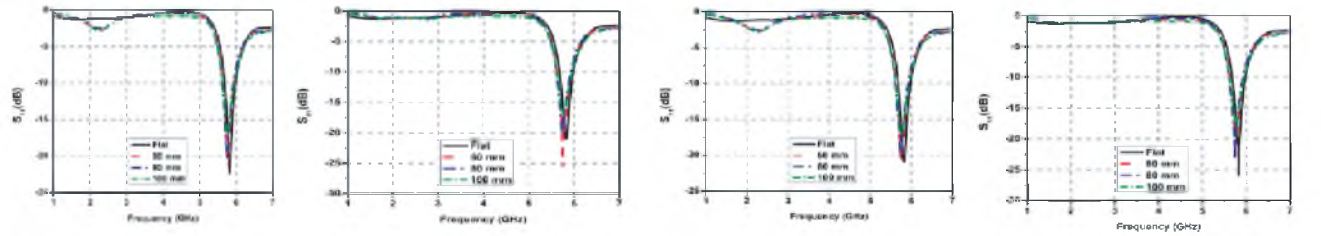

(a) (b) (c) (d)

Figure 14. S_{11} under bending condition: (a) y-direction OFF state (simulation), (b) y-direction OFF state (measurement), (c) x-direction OFF state (simulation), (d) x-direction OFF state (measurement).

higher accuracy than the measurement results. The discrepancy is attributed to various variables, including utilization of Styrofoam, defects in manufacturing, and cable degradation. Additionally, the investigation explores the radiation patterns along the diameters. Figs. 15(a)–(f) demonstrate that the radiation pattern remains similar for both simulation and measurements in both the ON and OFF states.

5. ON-BODY MEASUREMENT

Considering that the antenna is specifically developed for close contact with the human body, the overall antenna performance in human proximity is explored. Fig. 16 illustrates the placement of the antenna on various parts of the body (lap, chest, and arm) to observe changes in dual-frequency behavior. The measured S_{11} values, displayed in Fig. 17 for both ON and OFF states, exhibit a satisfactory correlation with the simulation results. In addition, when the antenna is positioned onto a person's

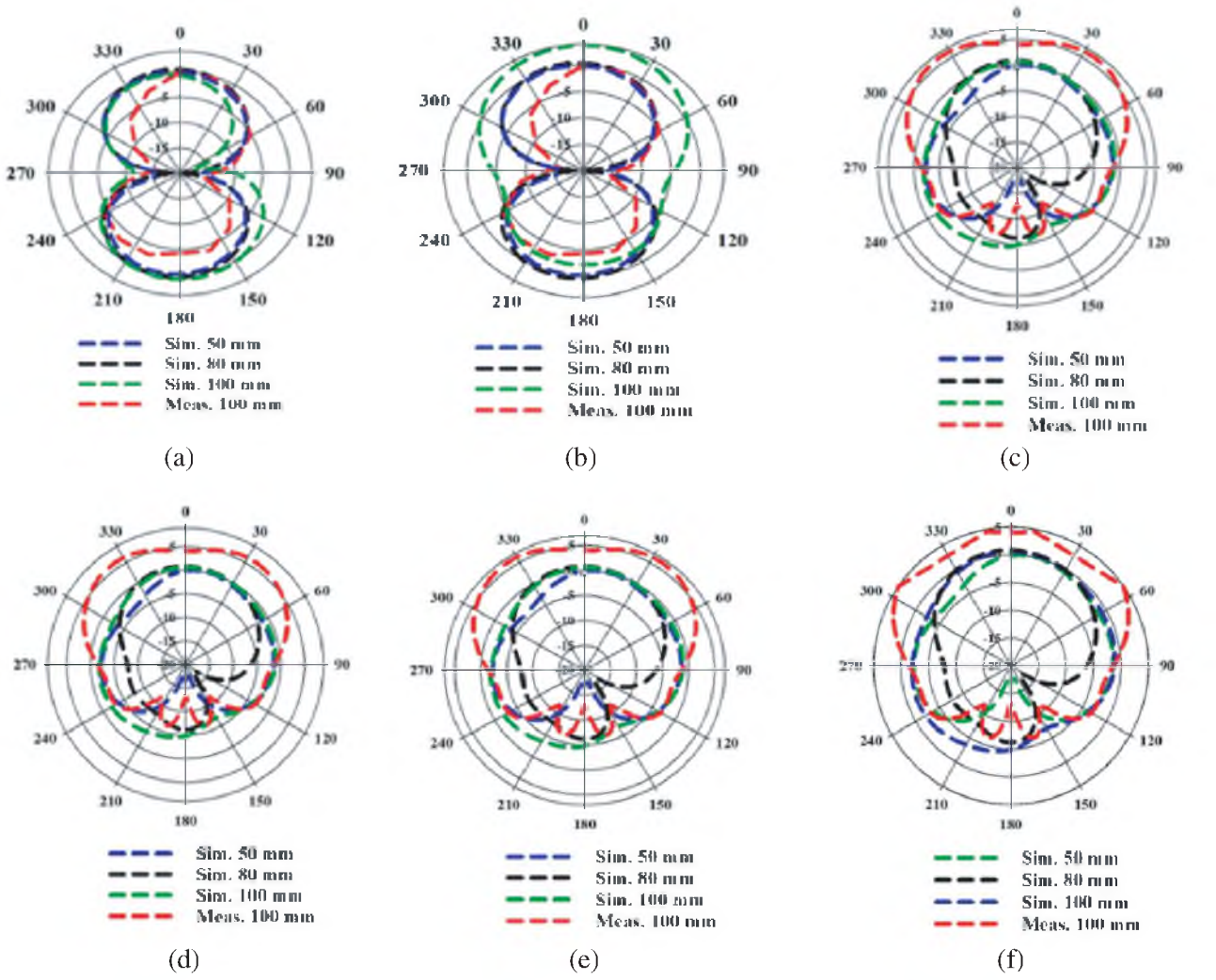

Figure 15. Radiation patterns under bending: (a) 2.4 GHz ON state (y-direction), (b) 2.4 GHz ON state (x-direction), (c) 5.8 GHz ON state (y-direction), (d) 5.8 GHz ON state (x-direction), (e) 5.8 GHz OFF state (y-direction), (f) 5.8 GHz OFF state (x-direction).

Figure 16. Antenna's position on various regions of the human body: (a) lap, (b) chest, (c) arm.

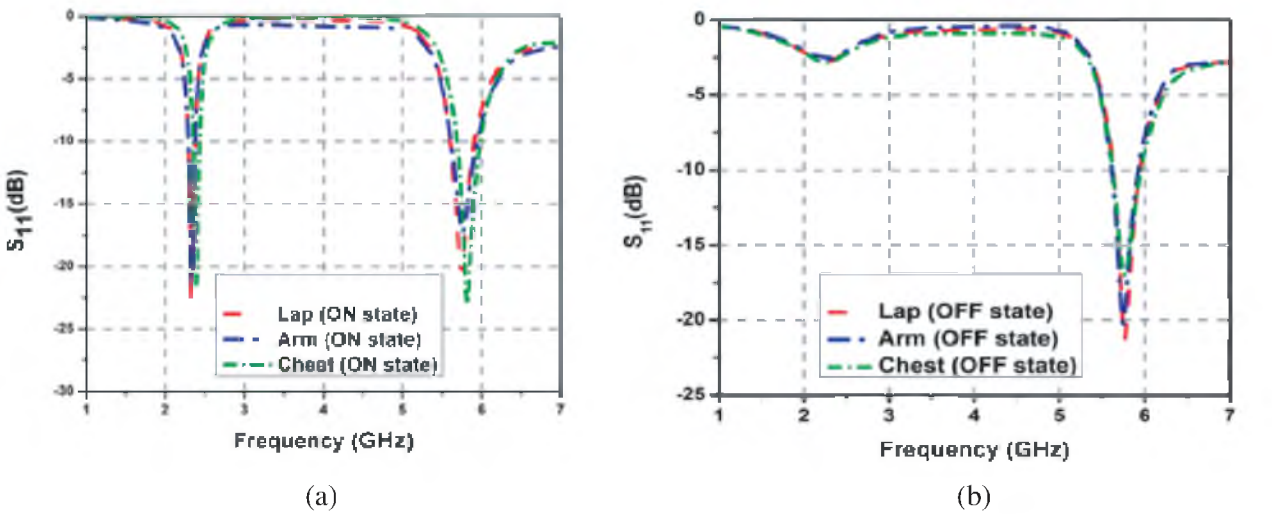

Figure 17. Comparison of measured S_{11} on various regions of the human body: (a) ON state, (b) OFF state.

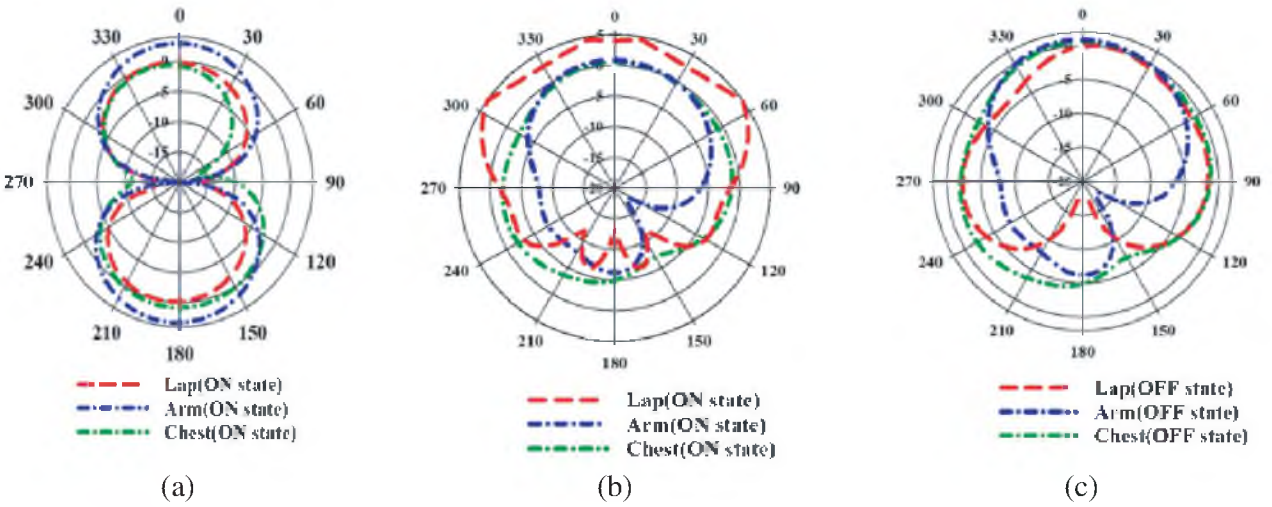

Figure 18. Radiation patterns on various regions of the human body: (a) 2.4 GHz (ON state), (b) 5.8 GHz (ON state), (c) 5.8 GHz (OFF state).

physique, the radiation patterns are recorded and presented in Fig. 18. These patterns demonstrate similarities between different body placements.

6. SAR ANALYSIS

Evaluating the SAR of an antenna while it is used within the human body is of utmost importance. The SAR level must be kept below specific thresholds to comply with standards set by the Federal Communications Commission (FCC) and the International Commission on Non-Ionizing Radiation Protection (ICNIRP). According to the FCC standard, the SAR should not surpass 1.6 W/kg for every gram of tissue, while the standard set by ICNIRP is 2 W/kg per 10 g of tissue [41, 42]. In the CST Microwave Studio^{TM} software, the IEEE C95.1 standard is used to calculate the SAR limits. These limits can be enhanced by using input power levels ranging from 25 mW to 100 mW. Fig. 19 illustrates the layers of a human body tissue model, and Table 2 provides the characteristics of a model of human

Table 2. Characteristics of a model of human tissue [34].

Level	Skin	Fat	Muscle	Bone
Dielectric Constant (F/m)	37.11	5.95	57.48	19.49
Density (kg/m^2)	2100	810	1041	1008
Conductivity (Ωm)	5.72	1.98	5.96	1.82
Thickness (mm)	3	6	19	15

Table 3. The antenna's SAR values for different input power levels.

Power (mW)	25		50		100		150	
Tissue weight in grams	1	10	1	10	1	10	1	10
SAR values (W/kg)								
2.4 GHz	0.66	0.29	0.82	0.58	0.41	0.18	1.16	0.46
5.8 GHz	0.23	0.25	0.45	0.37	0.44	0.16	0.99	0.63

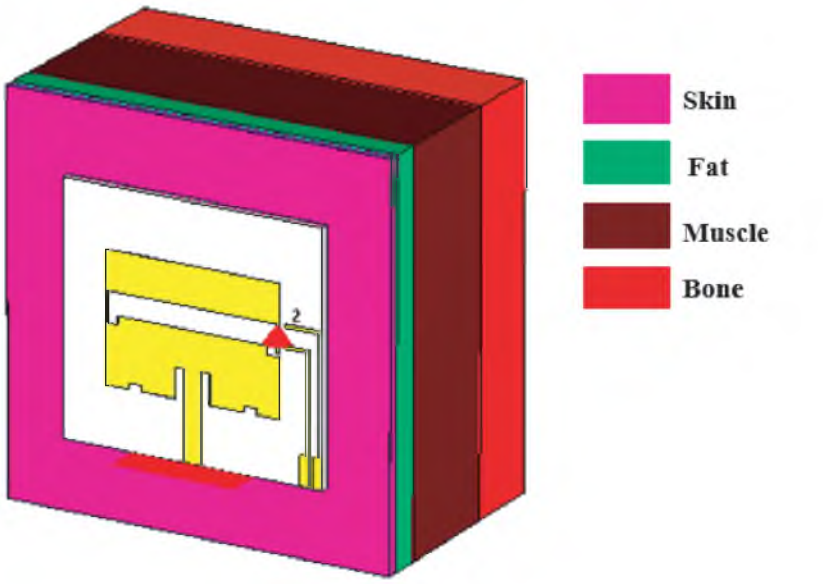

Figure 19. The simplified human body tissue model.

tissue.

The antenna's SAR values in the presence of human tissue weighing 1 g and 10 g, respectively, are illustrated in Table 3, adhering to the FCC and CNIRP standards. The input power levels of 25 mW to 150 mW were used for the measurements. To model the SAR values corresponding to the patch antenna's placement, which was at a 10 mm distance from the human phantom, an input power of 100 mW was selected based on the outcomes in the table. The antenna cannot be placed directly on bare skin and is instead positioned on the user's clothing, which has an approximate thickness of 10 mm. The resulting SAR values can be seen in Figs. 20(a) to (d). At 2.4 GHz, the SAR values for 1/10 g of human tissue are 0.411/0.177 W/kg respectively as depicted in Figs. 20(a) and (b). Similarly, at 5.8 GHz, the SAR values are 0.438/0.158 W/kg respectively as depicted in Figs. 20(c) and (d). These findings indicate that the achieved SAR levels in this study are comfortably below the standards established by the FCC and

Table 4. Assessment of performance of the designed antenna in comparison with prior work.

Ref.	Size (λ_0^3)	Material (ε_r)	Reconfigurability type (Number of freq. bands achieved)	Number of (switches used)	Freq. (GHz)	SAR (W/kg)	Gain (dBi)	Efficiency (%)
[9]	0.56 × 0.47 × 0.03 @ 1.8 GHz	PF4 Form (1.06)	Frequency (5)	1	1.82–3.79	–	1.07–7.37	29.8–93.7
[27]	0.41 × 0.29 × 0.003 (@ 3.5 GHz)	Rogers (2.2)	Frequency (2)	2	2.05–10.7	–	2.02–5.31	83.5–87.3
[29]	0.71 × 0.66 × 0.0012 (@ 2.4 GHz)	Rogers (3)	Frequency (2)	1	2.45, 3.3	0.29	3, 6.4	–
[30]	0.13 × 0.13 × 0.0001 (@ 2.45 GHz)	Rogers (3.55)	Frequency (3)	5	1.575, 2.45, 5.2	0.16, 0.52, 1.13	3.26, 3.47, 4.04	82, 85, 88
[43]	0.19 × 0.04 × 0.008 (@ 2.45 GHz)	Denim (1.68)	Frequency (2)	1	2.45, 5.25	–	3.55, 3.17	–
[44]	0.23 × 0.198 × 0.018 (@ 3.5 GHz)	Polyester (3.4)	Frequency (4)	5	2–6	–	–	–
[45]	0.82 × 0.82 × 0.0016 (@ 2.45 GHz)	Thick Felt (1.3)	Frequency/ Polarization (2)	4	2.45, 5.8	0.042, 0.09	5.93, 6.02	55.6, 72.5
[46]	π × 0.2242 × 0.016 (@ 2.45 GHz)	F4B (2.55)	Frequency (2)	3	2.45, 5.8	17.8, 4	0.36, 5.06	–
This work	**0.33 × 0.35 × 0.012 (@ 2.4 GHz)**	**Rogers (3)**	**Frequency (2)**	**1**	**2.4, 5.8**	**0.18, 0.16**	**4.84, 6.01**	**92.5, 91.8**

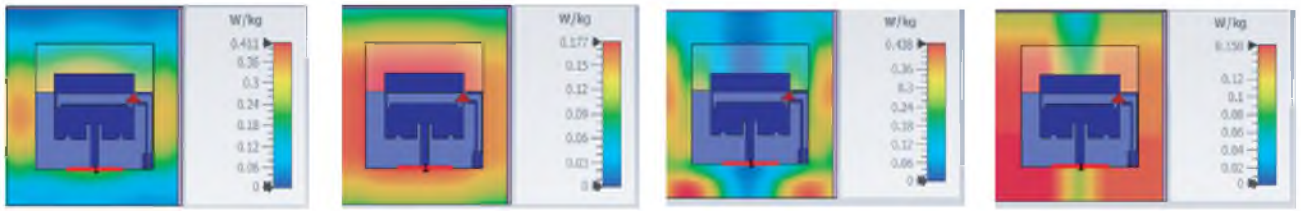

(a) (b) (c) (d)

Figure 20. SAR values (100 mW input power): (a) 2.4 GHz (1 g), (b) 2.4 GHz (10 g), (c) 5.8 GHz (1 g), (d) 10 g at 5.8 GHz (10 g).

ICNIRP. The novelty of the proposed antenna is highlighted in Table 4, which presents a comparison with previous research. The comparison clearly indicates that the suggested antenna is compact in size, with acceptable low SAR levels, and delivers excellent gain and efficiency across all operational frequency bands. Moreover, the antenna employs only a single switch, reducing its complexity.

7. CONCLUSION

This paper introduces a wearable patch antenna for WBAN applications which incorporates a PIN diode to enable frequency reconfiguration. The proposed antenna is fabricated on a semi-flexible Rogers Duroid RO3003^{TM} with compact dimensions of $0.33\lambda_0 \times 0.35\lambda_0 \times 0.012\lambda_0$. The antenna utilizes a U-shaped slot in an inverted configuration, Through the inclusion of a PIN diode to facilitate switching between the ON and OFF states, the antenna can function as either single-band (ISM 5.8 GHz) or dual-bands

(ISM 2.4 GHz and 5.8 GHz) by design. In the ON state, the antenna provides an impedance bandwidth of 3.8% at 2.4 GHz and 5.2% at 5.8 GHz, while the OFF state offers a 5.2% impedance bandwidth at the upper band. The radiation characteristics are bi-directional at 2.4 GHz and directional at 5.8 GHz. When in the ON state, the antenna achieves a peak gain of 4.84 dBi and 5.87 dBi, with total efficiencies of 92.5% and 92.7% at 2.4 GHz and 5.8 GHz, respectively. In the OFF state, the antenna exhibits a peak gain of 6.01 dBi and a total efficiency of 91.8% at 5.8 GHz. The antenna's functionality was evaluated using a human tissue model, and the SAR values were measured to determine its suitability for WBAN applications. At 2.4 GHz, the SAR values for 1/10 g of human tissue are 0.411/0.177 W/kg, respectively. Similarly, at 5.8 GHz, the SAR values are 0.438/0.158 W/kg, respectively. As a result, the suggested antenna provides the potential for WBAN applications. It possesses a compact size, adheres to low SAR limits, exhibits good gain and efficiency across all operating bands, and offers the advantage of requiring only a single switch, reducing its complexity compared to previous designs.

ACKNOWLEDGMENT

This work was supported by the Ministry of Higher Education (MoHE) under Fundamental Research Grant Scheme FRGS/1/2020/TK0/UTHM/02/44.

REFERENCES

1. Yaghoubi, M., K. Ahmed, and Y. Miao, "Wireless Body Area Network (WBAN): A survey on architecture, technologies, energy consumption, and security challenges," *J. Sens. Actuator Networks*, Vol. 11, No. 4, 2022.
2. Monirujjaman Khan, M., J. Hossain, K. Islam, N. S. Ovi, M. N. A. Shovon, M. I. Abbasi, and S. Bourouis, "Design and study of an mmwave wearable textile based compact antenna for healthcare applications," *Int. J. Antennas Propag.*, Vol. 2021, 6506128, 2021.
3. Li, Y., L. Zheng, and X. Wang, "Flexible and wearable healthcare sensors for visual reality health-monitoring," *Virtual Real. Intell. Hardw.*, Vol. 1, No. 4, 411–427, 2019.
4. Zhu, X.-Q., Y.-X. Guo, and W. Wu, "A compact dual-band antenna for wireless body-area network applications," *IEEE Antennas Wirel. Propag. Lett.*, Vol. 15, 98–101, 2016.
5. Yan, S., P. J. Soh, and G. A. E. Vandenbosch, "Wearable dual-band composite right/left-handed waveguide textile antenna for WLAN applications," *Electron. Lett.*, Vol. 50, No. 6, 424–426, 2014.
6. H. Savcı and F. Kaburcuk, "FDTD-based SAR calculation of a wearable antenna for wireless body area network devices," *Int. J. Microw. Wirel. Technol.*, 1–7, 2022.
7. Soh, P. J., G. Vandenbosch, S. L. Ooi, and N. Husna, "Wearable dual-band Sierpinski fractal PIFA using conductive fabric," *Electron. Lett.*, Vol. 47, 365–367, 2011.
8. Ge, L. and K.-M. Luk, "Frequency-reconfigurable low-profile circular monopolar patch antenna," *IEEE Trans. Antennas Propag.*, Vol. 62, No. 7, 3443–3449, 2014.
9. Dang, Q. H., S. J. Chen, D. C. Ranasinghe, and C. Fumeaux, "A frequency-reconfigurable wearable textile antenna with one-octave tuning range," *IEEE Trans. Antennas Propag.*, Vol. 69, No. 12, 8080–8089, 2021.
10. Puskely, J., M. Pokorny, J. Lacik, and Z. K. Raida, "Wearable disc-like antenna for body-centric communications at 61 GHz," *IEEE Antennas Wirel. Propag. Lett.*, Vol. 14, 1490–1493, 2015.
11. Musavand, A., Y. Zehforoosh, H. Ojaroudi, and N. Ojaroudi, "A compact UWB slot antenna with reconfigurable band-notched function for multimode applications," *Appl. Comput. Electromagn. Soc. J.*, Vol. 31, No. 1, 14–18, 2016.
12. Shah, S. M., M. F. M. Daud, Z. Z. Abidin, F. C. Seman, S. A. Hamzah, N. Katiran, and F. Zubir, "Frequency reconfiguration mechanism of a PIN diode on a reconfigurable antenna for LTE and WLAN applications," *Int. J. Electr. Comput. Eng.*, Vol. 8, No. 3, 1893–1902, 2018.
13. Tawk, Y., J. Costantine, and C. G. Christodoulou, "A varactor-based reconfigurable filtenna," *IEEE Antennas Wirel. Propag. Lett.*, Vol. 11, 716–719, 2012.

14. Ramli, M., M. Z. Abd Aziz, M. A. Othman, H. Nornikman, M. Azizi, S. Azlan, A. Dahalan, and H. Sulaiman, "Design of Sierpinski gasket fractal antenna with slits for multiband application," *J. Teknol.*, Vol. 78, 123–128, 2016.
15. Yang, S., C. Zhang, H. K. Pan, A. E. Fathy, and V. K. Nair, "Frequency-reconfigurable antennas for multiradio wireless platforms," *IEEE Microw. Mag.*, Vol. 10, No. 1, 66–63, Feb. 2009.
16. Shah, I. A., S. Hayat, A. Basir, M. Zada, S. A. A. Shah, S. Ullah, and S. Ullah, "Design and analysis of a hexa-band frequency reconfigurable antenna for wireless communication," *AEU — Int. J. Electron. Commun.*, Vol. 98, 80–88, 2019.
17. Ismail, M. F., M. K. A. Rahim, M. R. Hamid, H. A. Majid, A. H. Omar, L. O. Nur, and B. S. Nugroho, "Dual-band pattern reconfigurable antenna using electromagnetic band-gap structure," *AEU — Int. J. Electron. Commun.*, Vol. 130, 153571, 2021.
18. Reji, V. and C. T. Manimegalai, "V-shaped long wire frequency reconfigurable antenna for WLAN and ISM band applications," *AEU — Int. J. Electron. Commun.*, Vol. 140, 153937, 2021.
19. Pant, A., L. Kumar, R. D. Gupta, and M. S. Parihar, "Investigation on non-linear aspects of pattern reconfigurable hexagon shaped planar loop antenna," *IET Microwaves, Antennas Propag.*, Vol. 13, No. 8, 1158–1165, 2019.
20. Rahmani, F., N. Touhami, A. Kchairi, and N. Taher, "Circular Planar Antenna With Reconfigurable Radiation Pattern using PIN diodes," Vol. 46, 760–765, 2020.
21. Palsokar, A. A. and S. L. Lahudkar, "Frequency and pattern reconfigurable rectangular patch antenna using single PIN diode," *AEU — Int. J. Electron. Commun.*, Vol. 125, 153370, 2020.
22. Jin, G., L. Li, and W. Wang, "A wideband polarization reconfigurable antenna based on optical switches and C-shaped radiator," *2019 International Conference on Microwave and Millimeter Wave Technology (ICMMT)*, 1–3, May 2019.
23. Kovitz, J. M., H. Rajagopalan, and Y. Rahmat-Samii, "Design and implementation of broadband MEMS RHCP/LHCP reconfigurable arrays using rotated E-shaped patch elements," *IEEE Trans. Antennas Propag.*, Vol. 63, No. 6, 2497–2507, Jun. 2015.
24. Hu, Z., S. Wang, Z. Shen, and W. Wu, "Broadband polarization-reconfigurable water spiral antenna of low profile," *IEEE Antennas Wirel. Propag. Lett.*, Vol. 16, 1377–1380, 2017.
25. George, U. and F. Lili, "A simple frequency and polarization reconfigurable antenna," *Electromagnetics*, Vol. 40, No. 6, 435–444, 2020.
26. Chen, S., D. Ranasinghe, and C. Fumeaux, "A robust snap-on button solution for reconfigurable wearable textile antennas," *IEEE Trans. Antennas Propag.*, Vol. 66, No. 9, 4541–4551, 2018.
27. Hussain, N., W. A. Awan, S. I. Naqvi, A. Ghaffar, A. Zaidi, S. A. Naqvi, A. Iftikhar, and X. J. Li, "A compact flexible frequency reconfigurable antenna for heterogeneous applications," *IEEE Access*, Vol. 8, 173298–173307, 2020.
28. Salleh, S. M., M. Jusoh, A. H. Ismail, M. R. Kamarudin, P. Nobles, M. K. A. Rahim, T. Sabapathy, M. N. Osman, M. I. Jais, and P. J. Soh, "Textile antenna with simultaneous frequency and polarization reconfiguration for WBAN," *IEEE Access*, Vol. 6, 7350–7358, 2017.
29. Saeed, S. M., C. A. Balanis, C. R. Birtcher, A. C. Durgun, and H. N. Shaman, "Wearable flexible reconfigurable antenna integrated with artificial magnetic conductor," *IEEE Antennas Wirel. Propag. Lett.*, Vol. 16, 2396–2399, 2017.
30. Kanagasabai, M., P. Sambandam, G. N. A. Mohammed, N. M. Dinesh, M. S. Morais, A. Viswanathan, S. K. Palaniswamy, and A. Shrivastav, "On the design of frequency reconfigurable tri-band miniaturized antenna for WBAN applications," *AEU — Int. J. Electron. Commun.*, Vol. 127, 153450, 2020.
31. Sandeep, D. R., N. Prabakaran, B. T. P. Madhav, K. L. Narayana, and Y. P. Reddy, "Semicircular shape hybrid reconfigurable antenna on Jute textile for ISM, Wi-Fi, Wi-MAX, and W-LAN applications," *Int. J. RF Microw. Comput. Eng.*, Vol. 30, No. 11, e22401, 2020.
32. Ahmad, A., F. Faisal, S. Ullah, and D.-Y. Choi, "Design and SAR analysis of a dual band wearable antenna for WLAN applications," *Appl. Sci.*, Vol. 12, No. 18, 9218, 2022.

33. Hirtenfelder, F., "Effective antenna Simulations using CST MICROWAVE STUDIO (R)," 239, 2007.
34. Musa, U., S. M. Shah, H. A. Majid, Z. Z. Abidin, M. S. Yahya, S. Babani, and Z. Yunusa, "Recent advancement of wearable reconfigurable antenna technologies: A Review," *IEEE Access*, Vol. 10, 121831–121863, 2022.
35. Skyworks, 'SMP1321 Series: Low Capacitance, Plastic Packaged PIN Diodes," Skyworks Solut., 2019.
36. Roy, A., S. Bhunia, D. Sarkar, P. Sarkar, and S. Chowdhury, "Compact multi frequency strip loaded microstrip patch antenna with spur-lines," *Int. J. Microw. Wirel. Technol.*, Vol. 9, 1–11, 2016.
37. Aneesh, M., J. A. Ansari, and A. Singh, "Analysis of S-shape microstrip patch antenna for bluetooth application," *Int. J. Sci. Res. Publ.*, Vol. 3, No. 11, 2013.
38. Pandey, V. K. and B. Vishvakarma, "Theoretical analysis of linear array antenna of stacked patches," *Indian J. Radio Sp. Phys.*, Vol. 34, 125–130, 2005.
39. Meshram, M., B. Vishvakarma, and M. Meshramy, "Gap-coupled microstrip array antenna for wide-band operation Gap-coupled microstrip array antenna for wide-band operation," *Int. J. Electron.*, Vol. 88, 2001.
40. Musa, U., S. Babani, Z. Yunusa, and A. S. Ali, "Bandwidth enhancement of microstrip patch antenna using slits for 5G mobile communication networks," *2020 International Symposium on Antennas and Propagation (ISAP)*, 559–560, Jan. 2021.
41. "Guidelines for limiting exposure to time-varying electric magnetic, and electromagnetic fields (up to 300 GHz)," *Health Phys.*, Vol. 74, No. 5, 494–522, Radiation, ICNIRP (International Commission on Non-Ionizing Protection), 1998.
42. "IEEE Standard for Safety Levels with Respect to Human Exposure to Radio Frequency Electromagnetic Fields, 3 kHz to 300 GHz," *IEEE Std C95.1*, 1999 Ed., 1–83, Apr. 1999.
43. Tahir,, F. A. and A. Javed, "A compact dual-band frequency-reconfigurable textile antenna for wearable applications," *Microw. Opt. Technol. Lett.*, Vol. 57, No. 10, 2251–2257, 2015.
44. Muduli, A., M. Kanneboina, K. Mudumunthala, and S. Valluri, "A reconfigurable wearable antenna for mid band 5G applications," *J. Phys. Conf. Ser.*, Vol. 1921, 12051, 2021.
45. Fang, S., L. Zhou, and X. Jia, "Dual-band and dual-polarized circular patch textile antenna for on-/off-body WBAN applications," *IET Microwaves, Antennas Propag.*, Vol. 14, 2020.
46. Tong, X., C. Liu, X. Liu, H. Guo, and X. Yang, "Dual-band on-/off-body reconfigurable antenna for Wireless Body Area Network (WBAN) applications," *Microw. Opt. Technol. Lett.*, Vol. 60, No. 4, 945–951, 2018.